AGU PUBLICATIONS

JGR

Journal of Geophysical Research: Space Physics

RESEARCH ARTICLE

10.1002/2013JA019459

Key Points:
- Midnight MFD is an efficient mechanism to generate a very thin current sheet
- The MFD model is subject to the adiabatic constraint
- The MFD causes the equatorward motion of field-aligned currents

Correspondence to:
M.-S. Hsieh,
mhsieh2@alaska.edu

Citation:
Hsieh, M.-S., and A. Otto (2014), The influence of magnetic flux depletion on the magnetotail and auroral morphology during the substorm growth phase, *J. Geophys. Res. Space Physics*, *119*, 3430–3443, doi:10.1002/2013JA019459.

Received 16 SEP 2013
Accepted 23 MAR 2014
Accepted article online 27 MAR 2014
Published online 12 MAY 2014

The influence of magnetic flux depletion on the magnetotail and auroral morphology during the substorm growth phase

M.-S. Hsieh[1] and A. Otto[1]

[1]Geophysical Institute, University of Alaska Fairbanks, Fairbanks, Alaska, USA

Abstract The substorm growth phase is characterized by the equatorward motion of the growth phase arc close to or even into the region of diffuse aurora characteristic for a dipolar magnetic field. The presented study examines changes of the near-Earth current sheet and of the mapping of magnetotail feature into the auroral ionosphere based on midnight magnetic flux depletion (MFD) in the near-Earth tail. Midnight MFD is caused by sunward convection to replenish magnetic flux that is eroded on the dayside by magnetic reconnection during periods of southward interplanetary magnetic field. The results demonstrate that MFD causes the formation of a very thin current sheet in the near-Earth tail. It is found that the removal of magnetic flux in the near-Earth tail causes a contraction of the ionospheric footpoints of this tail region such that all of the mapped magnetotail structures move equatorward by about 2 to 3°. The thin current layer is mapped into the region where magnetic flux is strongly depleted and in close proximity with strong and narrow regions 1 and 2 sense field-aligned currents. The ionospheric maps show a sharp transition between the dipole and stretched magnetic field and an evolution of thinning and convergent motion of field-aligned currents in the late growth phase. The results are obtained without loading of magnetic flux and energy into the tail lobes, demonstrating that many typical growth phase properties can be attributed to the depletion of near-Earth closed magnetic flux.

1. Introduction

The growth phase of substorms is generally believed to be initialed by the southward turning of interplanetary magnetic field (IMF) and the erosion of magnetic flux at dayside magnetopause through magnetic reconnection [*McPherron et al.*, 1973]. The duration of growth phase is typically about 30 min to 1 h. In this stage, open magnetic flux is accumulated in the magnetotail lobes which serves as a reservoir of the magnetic energy transferred from solar wind. The stored magnetic energy is released after the onset of the substorm expansion phase; however, the trigger mechanism of substorm onset and the physics of the substorm growth phase is still under debate. Several magnetotail properties are characteristic for the growth phase, such as the increase of the lobe magnetic field, the enhancement of crosstail current, and the thinning of current sheet (CS) [*Sanny et al.*, 1994; *Wang et al.*, 2004; *Petrukovich et al.*, 2007]. Particularly the evolution of a thin CS is of major importance to understand the mechanism that leads to the expansion phase onset [*Schindler and Birn*, 1993; *Birn et al.*, 1998; *Lee et al.*, 1998]. The thin CS is often observed within the radial distance at about 15 R_E with a thickness decreasing from several Earth radii down to hundreds of kilometers [*Sergeev et al.*, 1990; *Baker et al.*, 1993; *Asano et al.*, 2003]. In major substorms, a strongly distorted and stretched magnetotail can be seen near the geosynchronous station (~6.6 R_E) at an hour earlier of onset [*Kokubun and McPherron*, 1981], and a reduction of the dipolar field at geosyncronous distances is typical for the substorm growth phase.

The evolution of magnetotail is slow during the growth phase, and the associated tail convection is considered as a quasi-static process. Early ideas that the dayside reconnection can launch fast rarefaction waves which propagate into the magnetotail and facilitate sunward convection go back to *Mozer* [1971], *Coroniti and Kennel* [1973], *Coroniti* [1985], and *Kan* [1990]. The associated magnetic flux transport can balance the dayside reconnection and depletes the tail region of closed magnetic flux. *Erickson and Wolf* [1980] suggested that a steady, lossless, and adiabatic earthward convection in the magnetotail would lead to a pressure catastrophe because the large flux tube entropy of flux tube convected from the midtail into the near-Earth region implies a strong increase of thermal pressure during the convection and thereby leads to a strong force imbalance. In other words, magnetic flux tubes are likely to convect and divert around the Earth

mostly along contours of constant flux tube entropy. This slow adiabatic convection is a major constraint of the evolution of the magnetotail during the growth phase, which confines the depletion of magnetic flux in the tail to a region of particular flux tube entropy.

Auroral breakups of the preexisting equatorward auroral arc are widely described as the onset of an auroral substorm [*Akasofu*, 1964]. During the growth phase, auroral arcs are observed moving equatorward close to or even into the region of diffuse aurora. *Clausen et al.* [2012] suggested that the equatorward drift of auroral arcs is likely a result of the addition of open magnetic flux to the polar cap through the dayside reconnection, leading to an expansion of the region 1 current that moves toward lower latitudes. In this paper, we demonstrate that the equatorward motion of the field-aligned currents can be caused by the removal of closed tail magnetic flux, which is associated with the formation of thin CS even in the absence of any external compressions of the open magnetic flux.

We have proposed a model of CS thinning based on midnight magnetic flux depletion (MFD) which is caused by sunward convection to replenish dayside magnetic flux to balance magnetic reconnection during periods of southward IMF [*Otto et al.*, 2014]. An aspect of the model is the constraint imposed by adiabatic magnetotail convection. Specifically, we examine the changes of the near-Earth magnetotail region mapped into the ionosphere based on the *Tsyganenko* [1996, hereafter denoted as T96] magnetic field model corrected by the requirement of magnetic flux conservation. Of specific interest are the changes in magnetic flux, flux tube entropy, field-aligned currents, convection, and the size and location of the respective ionospheric footpoints of the magnetotail structure and properties. Both electron and ion isotropy boundaries are mapped into the ionosphere to provide a reference for the transition between dipolar and taillike field, auroral observations, and the ionospheric convection.

The results employ a three-dimensional mesocale magnetohydrodynamics (MHD) simulation of the near-Earth tail. A typical substorm growth phase is characterized by the removal of closed magnetic flux in the near-Earth tail and the loading of energy and magnetic flux into the tail lobes. However, in order to identify the influence of MFD, the presented study does not include the addition of lobe magnetic flux which can contribute to thin CS formation. By ignoring the presence of a lobe driver, this paper demonstrates that MFD is sufficient to generate the thin CS and to explain the typical equatorward motion of field-aligned currents during the substorm growth phase. A study including the additional influence of a lobe driver is considered separately.

Often and intuitively the stretching of the tail magnetic field and the equatorward expansion are believed to be associated with earthward or tailward flows in the plasma sheet. This notion is carefully examined and contradicted by a quantitative evaluation of the motion of flux tubes in the magnetotail in the presented model. This result implies that the removal of closed magnetic flux by the sunward flow leads to a major depletion of the closed magnetic field in the near-Earth region implying a significant reduction of the size of the ionospheric footpoints of this region, which is sufficient to explain the observed equatorward motion of the aurora during the growth phase. The MFD model is introduced in section 2, and the ionospheric maps of magnetotail structures are presented in section 3. In section 4, we quantitatively evaluate the radial displacement of flux tubes in the magnetotail. The results of this study are discussed and summarized in section 5.

2. Simulation Methods

2.1. Midnight Magnetic Flux Depletion (MFD) Model

In this paper, we first demonstrate key properties of the dynamical evolution of a thin CS based on the MFD model. This model is developed through *Otto* [1990] three-dimensional MHD code combined with T96 magnetic field model. Our simulation domain is within the region at $-45\,R_E \le x \le -5\,R_E$, $-15\,R_E \le y \le 15\,R_E$, $0\,R_E \le z \le 12\,R_E$ in Geocentric Solar Magnetospheric (GSM) coordinate as illustrated in Figure 1 which assumes symmetry between the Northern and Southern Hemispheres. Particular care is applied to the boundary conditions. At all boundaries except for the equatorial plane and the earthward boundary the velocity is assumed to be tangential. At the equatorial plane symmetry is implied. The sunward outflow condition is used to prescribe the rate of sunward magnetic flux transport and implemented such that the boundary condition does not cause artificial strong boundary current: At each boundary point a field line is traced into the simulation domain and, depending on its equatorial location in radial distance, an azimuthal divergent (from midnight) flow profile is assumed to specify the azimuthal velocity at the boundary point of

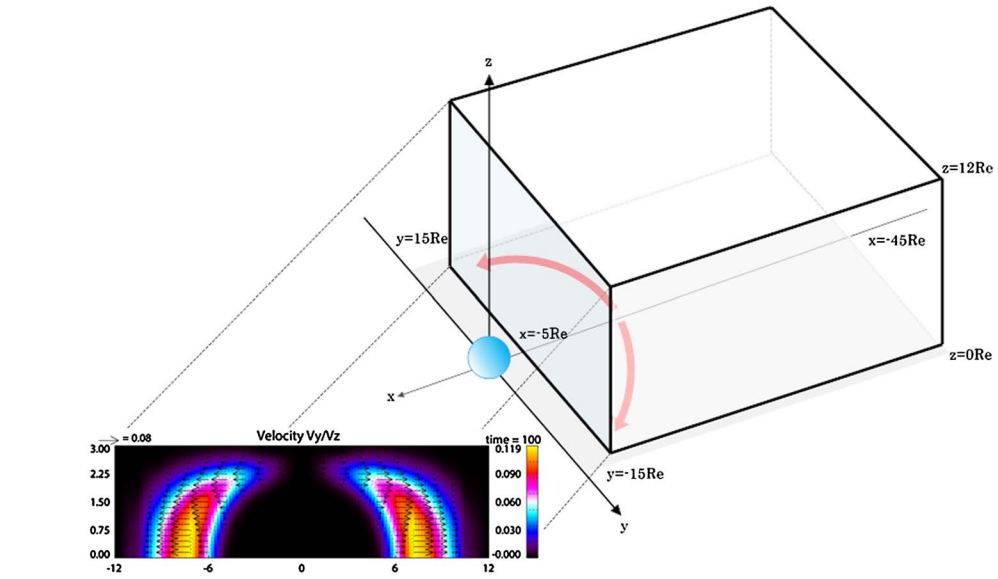

Figure 1. Sketch of the simulation box and the applied earthward boundary condition. A profile of the sunward divergent flow (the red arrows) is assumed in the equatorial plane. The rectangular panel shows the velocity mapped into the earthward boundary ($x = -5\,R_E$) at $t = 20$ min, in which the color shows the normal component and the arrow shows the tangential component of velocity.

the field line. This condition is dynamically updated during the simulation. We emphasize that this condition is applied only at the sunward boundary and there is no flow imposed in the equatorial plane. This sunward outflow is located at a radial distance of about 10 R_E (the red arrows in Figure 1) approximately consistent with adiabatic convection toward the dayside magnetopause. The rectangular panel in Figure 1 displays the velocity profile at the earthward boundary after the sunward divergent outflow is applied. Except for the specified sunward flow there is no normal component of the velocity at the earthward boundary.

Figure 2 shows the equilibrium crosstail current density (J_y) in the noon-midnight meridian plane which closely matches the current distribution from the T96 model. The initial configuration of the equilibrium magnetosphere is generated from ballistic relaxation technique described by *Hesse and Birn* [1993]. Note that our earthward boundary is at $x = -5\,R_E$; the maximum current density is initially located near the geosynchronous distances. The sunward flow is switched on in the MHD simulation at time $t = 0$ starting from the relaxed equilibrium state. All physical quantities in the simulation are normalized to the typical values; that is, the length scale is normalized by the Earth radius L_0 (1 R_E), the magnetic field is by B_0 (20 nT), the velocity is by the *Alfvén* velocity $V_A = B_0(\mu_0\rho_0)^{-1/2}$ ~430 km/s, the time is by *Alfvén* transit time $t_0 = L_0/V_A$ ~14.4 s, and the current density is by $B_0/(\mu_0 L_0)$ ~2.5 nA/m^2.

We have conducted a range of simulation cases with varying values of the sunward magnetic flux transport rate (potential). Here we will focus on a single case with an average potential of 40 kV to demonstrate fundamental properties of the thin CS formation and of the evolution of plasma sheet and field-aligned current properties mapped into the auroral ionosphere. A detailed comparison of the influence of different average potential values will be published separately. Also, the present results do not consider the influence of an increase of the lobe magnetic field or lobeward driving boundary condition in order to focus on the influence of the sunward flow alone.

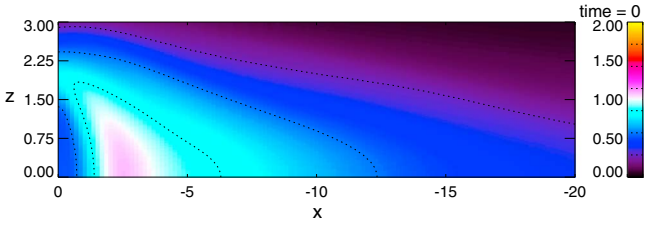

Figure 2. Equilibrium configuration of crosstail current density J_y in the noon-midnight meridian ($y = 0$).

2.2. Thin CS Formation

Figure 3 demonstrates the evolution of CS thinning during the growth phase. Figure 3 (top and bottom) presents the CS configuration at $t = 5$ and $t = 45$ min after the sunward divergent flow is

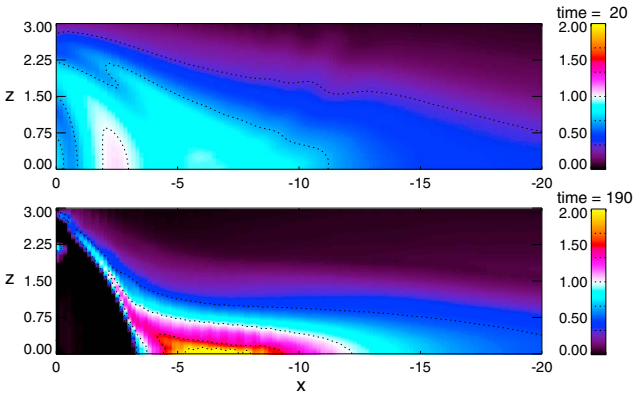

Figure 3. Same as Figure 2. J_y at (top) $t = 5$ min and (bottom) $t = 45$ min after the sunward outflow is switched on.

switched on. It is shown that the initially wide CS is significantly concentrated into a thin and strongly bifurcated current near the equatorial plane after 45 min. The thin CS has a peak current density ~9.6 nA/m^2 that is comparable with typical satellite observations [*Petrukovich et al.*, 2007; *Saito et al.*, 2011]. The earthward edge of the thin CS forms at about $x = -9\,R_E$ and extends to $x = -15\,R_E$, indicating that the thin CS structure is primarily confined to the near-Earth region. The CS thickness (estimated from the Harris sheet model) is initially 4.0 R_E and is reduced to 0.5 R_E after an hour (terminated time of the simulation). Figure 4 (left) shows the drastic change of the magnetic field strength in the equatorial plane during the midnight MFD process. The magnetic flux is significantly depleted down to values of B_Z ~1 nT in a large portion of the near-Earth plasma sheet consistent with the divergent (from midnight) slow convection at 10 R_E distance which forms in response to the earthward flow boundary condition. This slow divergent motion is the physical cause for the strong depletion of closed magnetic flux over the duration of the growth phase.

Figure 4 (right) presents the distribution of the azimuthal component j_ϕ of the current density in the equatorial plane. The figure illustrates the fairly wide section of the equatorial plane with thin CS formation. This is not unexpected in view of the relatively wide area with a strong depletion of the magnetic field B_z component. The enhanced plasma sheet current is seen well associated with the region where the magnetic field B_z is depleted, and it spans a relatively large area in azimuthal extent around ±40°. While the maximum

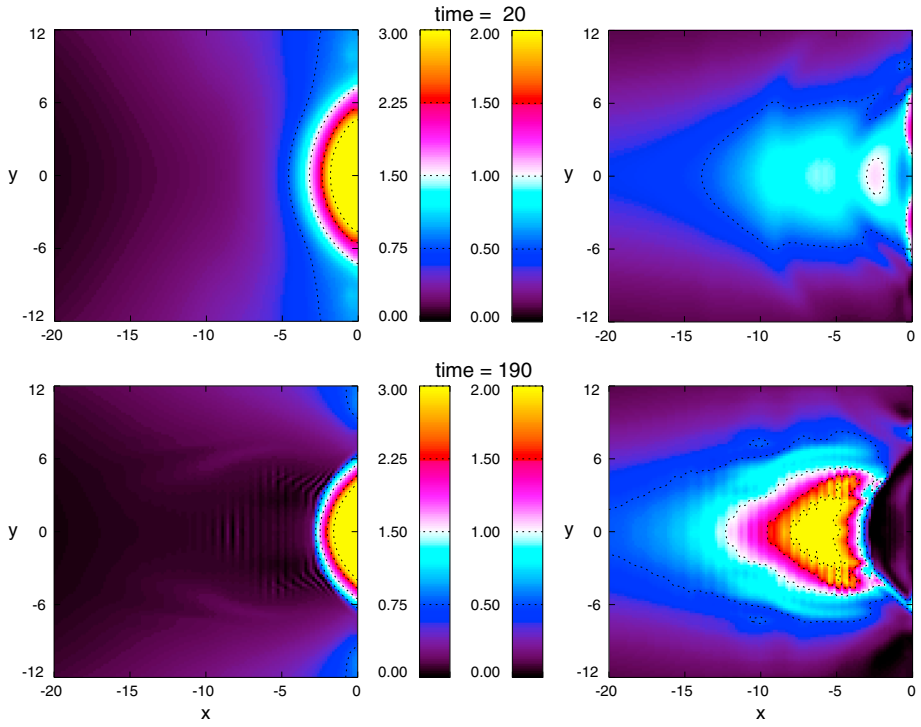

Figure 4. (left) Magnetic field strength B_z in the equatorial plane ($z = 0$), at (top) $t = 5$ min and (bottom) $t = 45$ min after the sunward outflow is switched on. (right) Same as Figure 4 (left) except for the azimuthal current density J_ϕ.

current density is close to or at the midnight meridian, a similarly large current density is found significant distances away from the midnight, such that reconnection onset may be easily possible at somewhat large distances from midnight (around 2200 LT ~ 0200 LT). We remark that these results are obtained by considering sunward convection only, i.e., without adding magnetic flux and energy to the lobes. In fact, the lobe magnetic field strength decreases by 10 to 20% from its initial value depending on location. Nevertheless, the results demonstrate the formation of a thin current sheet at a location and on a time scale that compare well with typical observations.

3. Near-Earth Tail Region Mapping

3.1. Mapping Method

Typical for substorm expansion onset is the auroral brightening and poleward expansion of the bright discrete aurora mostly simultaneous with major changes and fast convection in the magnetotail. During the growth phase a characteristic feature is the equatorward motion of the midnight aurora and particularly of the most equatorward discrete arc (growth phase arc) and of the poleward boundary of the aurora often associated with the closed magnetic field or plasma sheet boundary. This study examines the evolution of the ionospheric changes in the near-Earth magnetotail by quantitatively mapping flux tube properties of the thin CS from the earthward boundary into the ionosphere. Our mapping method is based on magnetic flux conservation combined with T96 magnetic field model. The T96 model is an empirical model based on the large number of satellite observations and on the modeling of magnetospheric current systems, which provides a statistical magnetic field parameterized by solar wind conditions. While our initial configuration is still close to the T96 model used for the initial input, the evolution close to the earthward boundary changes the strength and orientation of the magnetic field such that it is not anymore consistent with the initial T96 configuration. Worse, a simple unaltered use of the initial T96 model does not conserve magnetic flux because the magnetic field decreases in magnitude and changes in direction such that the earthward directed magnetic flux is much smaller than the corresponding flux into the ionosphere from the T96 model. In some regions of the earthward boundary the magnetic field is tilted strongly and actually shows a small negative B_x component. Thus, it is of major importance to include magnetic flux conservation in the mapping. The basic procedure is as follows. Attributing a certain ground truth to the statistical T96 mapping, the map in longitude is mostly preserved except for a small contraction factor measuring distance from midnight. This factor is 1 for our equatorward boundary and can be adjusted linearly going down with increasing latitude (reasonable values are between 0.7 and 0.9 at the poleward boundary). For the presented results the contraction factor is assumed to be 0.8 at the poleward boundary. Magnetic flux conservation implies that a smaller value (more contraction) would lead to reduced equatorial motion, while unmodified longitudinal map would lead to a larger amplitude of the equatorial displacement of footpoints. With the distribution of longitudinal coordinates for all boundary points the latitudinal width of each ionospheric grid cell (corresponding to a boundary cell of the simulation) is adjusted such that the flux into the ionosphere equals the flux out of our earthward boundary cell. Here the equatorward boundary of the simulation is kept fixed because changes are likely small at lower latitudes. Specifically, grid cell size in the ionosphere is converted from geographic/geomagnetic coordinates to length scales by

$$\frac{\Delta\lambda}{180^\circ}\pi = \frac{\Delta z_i}{1\,R_E}$$

$$\frac{\Delta\phi}{180^\circ}\pi = \frac{\Delta y_i}{1\,R_\lambda} = \frac{\Delta y_i}{1\,R_E\cos\lambda},$$

where we denote latitude as λ, longitude as ϕ, and y_i (also z_i) as the grid points at ionosphere. With magnetic flux conservation $\Phi_{msp} = \Phi_{io}$, B_0 is the normalization for the magnetic field and $B_{io}\cos\lambda$ is the magnetic flux normal to the ionosphere. Therefore, the latitudinal width of each ionospheric grid cell becomes

$$\Delta\lambda = A_i\frac{180^{\circ 2}}{\pi^2\Delta\phi\cos\lambda}$$

$$A_i = \frac{\Delta y\Delta z B_x B_0}{B_{io}},$$

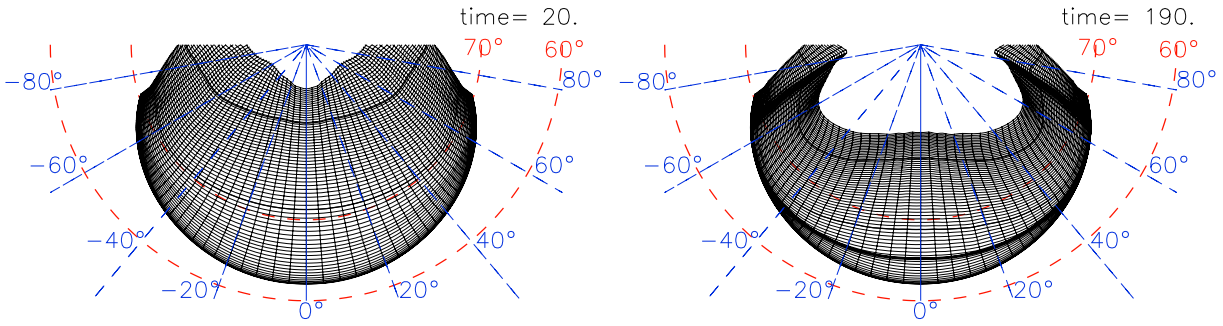

Figure 5. Grids of the earthward boundary mapped into the ionosphere. The ionospheric map at (left) $t = 5$ min and (right) $t = 45$ min. The red dashed lines mark the latitudes at 60° and 70°, and the blue dashed lines mark the longitudes from −80° to 80°. Only every third boundary grid is plotted here because the actual grid is too dense for a good illustration.

where Φ_{msp} (Φ_{io}) is the magnetic flux at the earthward boundary (ionosphere), B_{io} is the magnetic field strength at ionosphere surface $\sim 5.7 \times 10^4$ nT, A_i is the grid cell area at the ionosphere, $\Delta\lambda$ is the corrected latitude width, and i is the grid cell index. Note that B_x represents the magnetic field strength perpendicular to the cross section of the earthward boundary. For cells with negative $B_x \leq 0$, the ionospheric cross-sectional area is set to 0 consistent with no magnetic flux out of the simulation domain at this grid point.

Figure 5 shows the ionospheric maps where each grid point corresponds to a corresponding grid point at the earthward boundary of the simulation. Figure 5 (left and right) shows the map of the grid areas of the earthward boundary at $t = 5$ and $t = 45$ min (corresponding to the cases shown in Figure 3). The two thick lines are lines of the same constant z coordinate at the earthward boundary for the two plots and illustrate the equatorward motion of magnetospheric structures (with a fixed location in z at our earthward boundary) during the flux depletion. The cause for the equatorward expansion is in the region around 65° where many grid cells collapse to a zero area which maps to the region of divergent and sunward convection. The two thick lines in Figure 5 indicate that the equatorward motion is about 2° in latitude close to the equatorward boundary of the divergent convection and can be up to 4° in the more poleward regions of the aurora. Note that structures at higher latitudes move further than at the lower latitudes because of the decreasing cross-sectional area with increasing latitude. This also implies that the poleward plasma sheet boundary converges toward the most equatorward boundary structures. Employing this map as illustrated in Figure 5, all properties of the near-Earth tail can be mapped along magnetic field lines first into our earthward boundary and from there into the ionosphere.

The construction of this mapping is most reliable close to midnight because of the fairly strong dipolar character of field lines which constitute the equatorial boundary of our map. At larger distances from midnight and higher latitudes we expect increasing errors (1) because of the assumption to fix the mapping of the earthward edge of the equatorial plane (equatorward ionospheric boundary) by the original Tsyganenko field and (2) because of the assumption that the longitude of boundary grid coordinates is still mostly (except for the stretching factor) determined by the Tsyganenko field mapping. The disproportionate equatorward motion of the two reference lines at ±40° longitude from midnight is an indication of the larger mapping error away from midnight at higher latitudes. Also, mapping results at high latitudes and large distance from midnight are questionable because the corresponding field maps into one of the peripheral or lobe boundaries of the simulation. Mapping results in the remainder of this section are discussed only in a restricted region in latitude and around midnight.

3.2. Flux Tube Entropy

As a first example Figure 6 shows the ionospheric map of flux tube entropy defined as

$$H = \int \frac{p^{\frac{1}{\gamma}} \mathrm{d}s}{B},$$

where p is the thermal pressure, $\int \frac{\mathrm{d}s}{B}$ is the magnetic flux tube volume, and γ is $\frac{5}{3}$ for the adiabatic convection. The line integral of the flux tube entropy is integrated between the earthward boundary and the equatorial plane (or one of the other boundaries) and is then mapped into the ionosphere to demonstrate

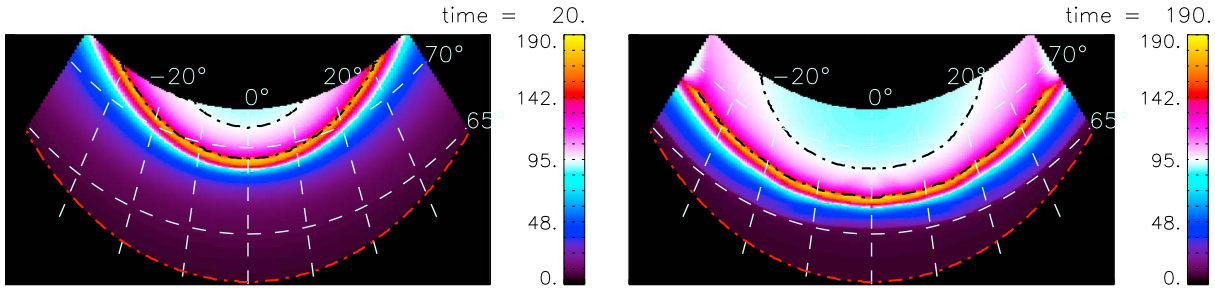

Figure 6. Ionospheric maps of flux tube entropy. The entropy map at (left) $t = 5$ min and (right) $t = 45$ min. The white dashed lines mark the longitudes and latitudes, where the map is within the range from −40° to 40° in longitude and 62° to 72° in latitude. The red dash-dotted line represents the intersection between the earthward boundary and the equatorial plane.

the change of plasma sheet boundary and boundaries mapped into ionosphere. The dash-dotted lines in Figure 6 indicate the location of the boundary edges of the simulation domain. The lower line (red) represents the intersection between earthward boundary and equatorial plane, the middle line (black) indicates the intersection between equatorial plane and tailward boundary, and the top line (black) represents the intersection between tailward and lobe boundary. These lines are also chosen to provide information on the endpoints of the field line integration.

We note that the flux tube entropy very close to the earthward boundary has a larger entropy error because of the limited length of magnetic field lines within the simulation domain. The dark region in the figure corresponds to the dipolar field with a very low entropy. The location of the near-Earth plasma sheet and midtail plasma sheet are the blue and yellow regions, respectively. The flux tube entropy decreases at higher latitudes, where magnetic field lines are connected to the tailward or lobeward boundary of the simulation domain and because the plasma pressure decreases for lobe field lines. The edge between equatorial and tailward boundary is located at $-45\ R_E$ in the simulation, and it moves from about 69 to 66.5° in latitude.

Although the simulation does not contain explicitly the open/closed boundary, the plasma sheet boundary has to be slightly equatorward of the intersection between tailward and lobeward boundary (about 1 to 2° poleward of the maximum field line entropy). This implies a motion from about 71 to 68° for the plasma sheet boundary. The near-Earth plasma sheet location is somewhat diffuse initially but is clearly indicated by the transition from dark to purple at later time indicative of a steeper gradient at this time. Overall, the figure demonstrates a clear equatorward motion of the entropy distribution by 2 to 3°, moving with a velocity about 100 m/s which is slow and comparable with the drift velocity of growth phase arcs found by *Aikio et al.* [2002]. Note that the equatorward motion of the open/close boundary is not caused by the magnetic flux added to the polar cap for the presented results. The removal of magnetic flux by the sunward divergent flow is sufficient to cause a realistic equatorward motion of typical tail properties.

3.3. Crosstail Plasma Sheet Current and Field-Aligned Currents

Figure 7 presents the ionospheric maps of crosstail plasma sheet current and is obtained by mapping the crosstail current density in the equatorial plane along field lines into the ionosphere using the outlined mapping procedure. The larger current close to our equatorward boundary (yellow) is likely a numerical artifact and is present only on the first few grid points (from the earthward boundary) of our simulation. It is shown that an initially wide CS develops into a thin intense current layer, located in the region where the magnetic

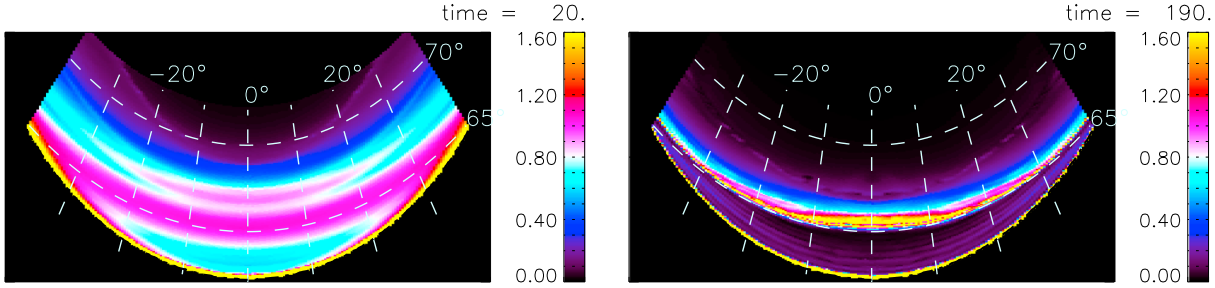

Figure 7. Same as Figure 6 except for the crosstail plasma sheet current.

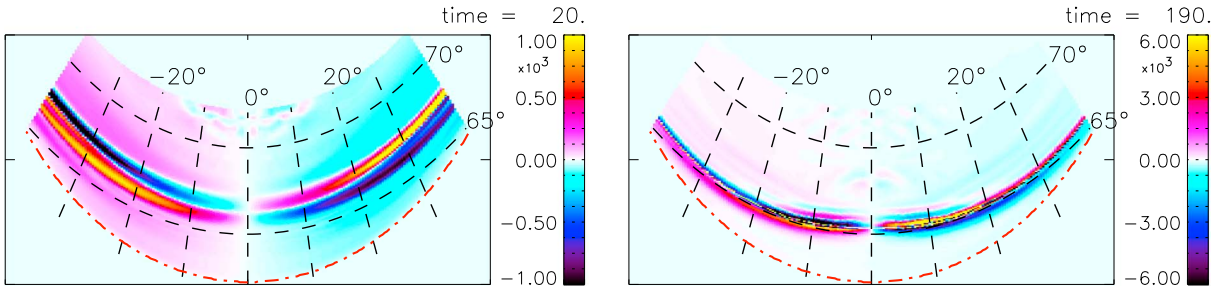

Figure 8. Same as Figure 6 except for the field-aligned currents.

flux is strongly depleted by the sunward divergent flow. The most intense current toward the end of the growth phase is confined to a narrow region about 1°.

Figure 8 shows the ionospheric maps of field-aligned currents (FACs). In the absence of divergent perpendicular currents along a magnetic field line, $\frac{J_{//}}{B}$ is a conserved quantity on magnetic flux tubes. Therefore the mapped field-aligned current $J_{//}$ is given by

$$J_{//} = \frac{J_{//msp}}{B_{msp}} B_{io},$$

where $J_{//msp}$ (B_{msp}) is the field-aligned current density (magnetic field) at the earthward boundary. It is shown that the intensity of field-aligned currents increases about sixfold and reaches 10^5 nA/m^2 in the late growth phase. The width of these intense FACs decreases to a rather small fraction of the initial distribution during the evolution. These strong field-aligned currents are directly associated with the region of the thin CS (also see Figure 7) because the sunward divergent flow bends the magnetic field lines, inducing the current density enhancement. The region 1 and region 2 currents (hereafter denoted as R1 and R2) are located in close proximity of the outer and inner boundaries of the return flow, respectively. The R2 current is located directly equatorward of the R1 and the intense crosstail current. The R1 current maps into the region of the most intense crosstail current.

Figure 8 presents an evolution of thinning and convergent motion of R1 and R2 currents during the growth phase. The spatial thinning of the field-aligned currents is likely also a result of the magnetic flux depletion. The strongly reduced B_z in the near-Earth tail requires a larger sunward flow in order to maintain an approximately constant flux transport rate ($E_y \sim v_x B_z$). This explains a narrower flow channel and an increasing convection velocity for consistency with an approximately constant magnetic flux transport rate (potential). Therefore, faster convection in a narrower channel can be expected in the ionosphere, consistent with more intense and narrower FAC distributions. Figure 8 also shows a clear equatorward motion of the R1 and R2 current system approximately consistent with the overall equatorward motion. The maximum R2 current moves by about 1° and the R1 current by about 2° equatorward. The distribution of field-aligned currents suggests that the growth phase arc is moving close to (or possibly into) the dipolar field region (typically characterized by diffuse aurora region) in the late growth phase.

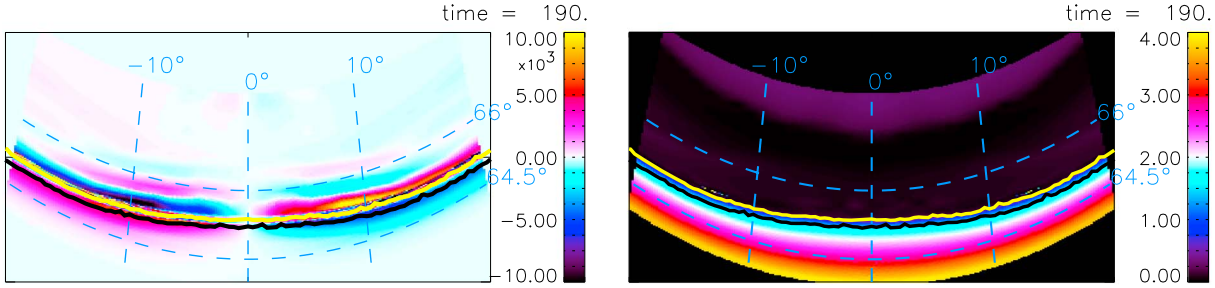

Figure 9. Ionospheric maps of isotropy boundaries. The yellow line presents 100 keV electron IB, and the black line presents 30 keV ion IB. The IBs superposed on the ionospheric maps of (left) field-aligned current density and (right) plasma sheet magnetic field strength. The maps are within the range from −20° to 20° in longitude and 64° to 68° in latitude.

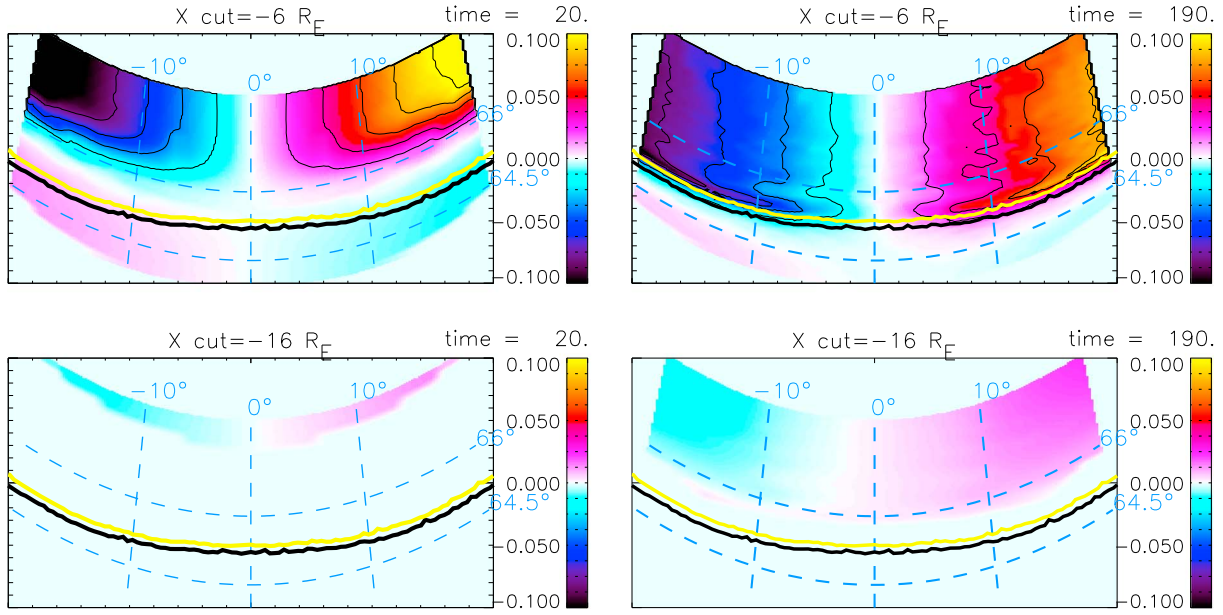

Figure 10. Ionospheric maps of isotropy boundaries superposed on the quasi-convection potential maps. Same as Figure 9 except for the quasi-potential. The quasi-potential when the x cut is at (top) $-6\,R_E$ and (bottom) $-16\,R_E$. The black contour lines indicate the constant quasi-potential.

3.4. Electron and Ion Isotropy Boundaries

Figures 9 and 10 show the 100 keV electron and 30 keV ion isotropy boundaries (IBs) mapped into the ionosphere superposed on the different ionospheric quantities. The IBs are the boundaries characterized by the adiabatic/chaostic motions as well as the regions characterized by particle precipitations. They are chosen by a threshold value of $R_c/r_{gi} \sim 8$ in the equatorial plane [*Sergeev and Tsyganeznko*, 1982], where R_c is the curvature radius of magnetic field lines and r_{gi} is the gyroradius of species. The 100 keV electron and 30 keV ion IB is represented as the yellow and black line, which is first mapped from the equatorial plane to the earthward boundary and then into the ionosphere.

Figure 9 (left and right) shows the IBs superposed on the ionospheric maps of field-aligned current density and magnetic field strength in the equatorial plane (or other boundary planes if the field line ends at any other simulation boundary). The magnetic field B_z in the equatorial plane is again determined by a field line integration from the earthward boundary into the tail. Figure 9 demonstrates that the electron IB maps almost exactly to the boundary between R1 and R2 currents and to the transition region from depleted to dipolar field, implying that the substorm growth phase is characterized by the equatorward motion of the auroral arc very close to the region of diffuse aurora characteristic for a dipolar magnetic field. The ion IB maps into the R2 current region and the dipolar field region about 0.3° equatorward of the electron IB. The transition between dipole/stretched field is at a latitude about 65°. Note that if the dipole field equation is considered, i.e., $L = 1/\cos^2\Lambda$ (Λ is invariant latitude), the dipole field boundary should trace to $L = 5.6$ in the magnetotail. However, the dipole field boundary is located at $L \sim 7.8$ in our simulation because of the reduction of the size of the ionospheric footpoints caused by the depleted magnetic flux in the near-Earth tail. The equatorward expansion, the location of the IBs, and the convergence and intensification of the R1 and R2 currents in the midnight region in the simulation as illustrated in Figure 9 provide a basic growth phase morphology that agrees well with typical properties of the auroral ionosphere [*Sergeev et al.*, 1993; *Yahnin et al.*, 1997; *Ohtani et al.*, 2010; *Sergeev et al.*, 2012].

A comparison of the location of the R1 current at the beginning and at the end of the growth phase indicates that the amplitude of the equatorward motion of the peak current location is slightly greater away from midnight. In fact, Figure 9 indicates that the actual location of the thin R1 current layer and of the IB is marginally further equatorward away from midnight (by $< 1/4°$); however, it may be interesting to note that the IB and the R1 current peak are at an almost constant magnetic latitude. This is somewhat counterintuitive because on a global scale one would expect the largest amplitude at midnight. We do not know if this result is an artifact of our mapping, but we note that for instance *Xing et al.* [2010] has several examples

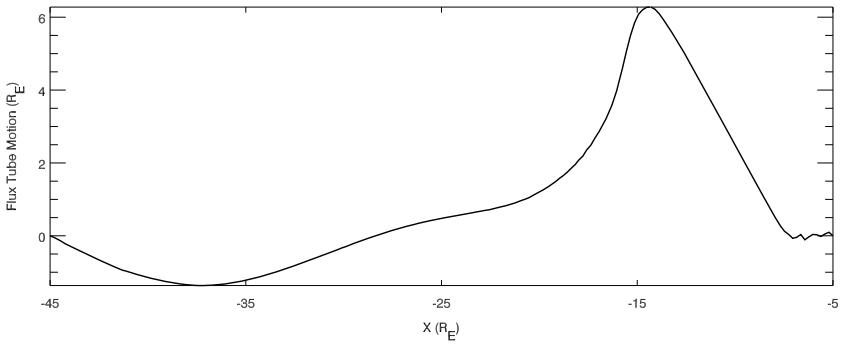

Figure 11. Flux tube motion in the midnight magnetotail based on the tracing of plasma elements in the equatorial plane. The *x* axis is the radial distance in the magnetotail within the simulation domain. The *y* axis is the flux tube deviations from the initial position, in which positive (negative) value corresponds to the earthward (tailward) motion.

where the growth phase or onset arc appears to be on an almost constant latitude within 15 to 30° from midnight. Note that the ion isotropy boundary corresponds well to the latitude of the maximum ion energy flux precipitation [*Newell et al.*, 1998].

Figure 10 shows the IBs superposed on the ionospheric maps of a quasi-convection potential. The potential calculation is a challenge and associated with several uncertainties because of a number of reasons: First, the electric field in the simulation is not a potential field. Most of the electric field in and close to the equatorial plane is associated with the change of the magnetic field $\partial B/\partial t$ and is therefore inductive. Second, we specify the outflow condition at the earthward boundary such that the electric field at the earthward boundary may have numerical artifacts. Third, the present model does not consider effects from finite ionospheric conductance. However, the changes in the magnetic field and the electric field are slow such that the electric field close to the earthward boundary may at least indicate some basic insight into changes of the ionospheric convection. We thus select the cut plane at $x = -6\,R_E$ which is close to the earthward boundary, and the quasi-potential is calculated from this plane and the equatorial plane between $-5\,R_E$ and $-6\,R_E$. In comparison, we select another cut at $x = -16\,R_E$ and the equatorial plane between $-5\,R_E$ and $-16\,R_E$ further away from the earthward boundary as shown in Figure 10 (bottom).

The black contour lines of Figure 10 indicate the constant potential which can also be represented as flow lines. It is shown that the overall convection propagates equatorward during the CS thinning. A clear pair of westward and eastward flows are seen away from the midnight, which is associated with the sunward divergent outflows. As shown in Figure 10 (top), the equatorward gradient of the quasi-potential steepens toward the end of growth phase (at ~65°), implying an increasing velocity of westward and eastward flows very close to the electron IB. In comparison with Figure 9, the flow channels are approximately coincident with the boundary of R1 and R2 currents. This result implies that the location of preonset arc is likely inside the channel of westward flows at the premidnight region, which is consistent with the ionospheric observation from *Bristow et al.* [2003]. It is also worth mentioning that the quasi-potential shows an apparent change with the choice of the *x* location of the plane to evaluate the electric field. Note that the quasi-potential is calculated from the cut and the equatorial section between the cut and $x = -5\,R_E$; i.e., a larger contribution of plasma sheet electric field is involved when the cut in *x* moves further tailward. Figure 10 (bottom) indicates that the overall plasma sheet potential is very low implying that plasma sheet convection is very slow. This result is expected because the magnetotail is subject to the slow adiabatic constraint and thereby the convection is slow, i.e., small convective electric fields consistent with many results of quasi-static evolution [*Erickson and Wolf*, 1980; *Schindler and Birn*, 1993; *Birn et al.*, 1998]. It is shown that the quasi-potential highly increases by a factor up to 10 when it is evaluated closer to Earth. The strong increase of quasi-potential is caused by the change of magnetic fields associated with significant inductive electric fields.

4. Flux Tube Motion in the Magnetotail

The previous section has demonstrated a clear equatorward motion of all of the magnetotail properties mapped into the ionosphere during the growth phase. The removal of magnetic flux results in the contraction of field line footpoints such that all of the mapped magnetotail structures move equatorward. Often the equatorward expansion is believed to be associated with earthward or tailward flows in the plasma sheet.

Here we quantitatively examine the motion of flux tubes in the magnetotail to provide further insight into the cause for the equatorward motion of ionospheric footpoints and the role of the magnetic flux depletion rather than a simple stretching of the magnetic field lines by divergent earthward convection.

Figure 11 shows the radial displacement of the footpoints of flux tubes (along x in the midnight) in the equatorial plane based on the tracing of plasma elements in the magnetotail from $t = 20t_A$ to $t = 190t_A$. Here a positive (negative) value corresponds to earthward (tailward) displacement of the flux tube along the radial direction. The radial displacement of equatorial footpoints is generally small and negligible except for a region between $-18\,R_E$ and $-8\,R_E$. The largest displacement is positive with a value of about $6\,R_E$ for an initial flux tube footpoint at about $-15\,R_E$. Closer to Earth the gradient is negative, implying converging motion along the x direction. Tailward the gradient is positive, implying that flux tubes starting tailward of the maximum have smaller displacements implying divergent motion or stretching. However, the stretching factor is only approximately 2 in the very limited region between $\sim -15\,R_E$ and $-18\,R_E$, i.e., the flux tube footpoints that are initially separated by $3\,R_E$ and are finally separated by about $6\,R_E$ at the end of the growth phase. Ignoring any crosstail variation, the stretching would only reduce the equatorial magnetic field by about 50%. While this is not negligible, it is insufficient to explain the actual reduction of the magnetic field in the midnight region which requires the divergent flow away from the midnight plane. Furthermore, the convergent motion of equatorial footpoints earthward of the maximum in Figure 11 implies an increase of the equatorial field at the associated location opposite to observational evidence and opposite to our model properties. This demonstrates that CS thinning and the mapping properties of our model cannot be attributed to simple notion of field line stretching which within our model is not negligible but an effect secondary to the divergent flow along the crosstail direction.

5. Discussion and Summary

This paper examines the evolution of the magnetotail and the associated ionospheric signatures for conditions that lead to a strong depletion of the near-Earth closed magnetic flux. The midnight MFD is caused by sunward convection to replenish magnetic flux which is eroded on the dayside magnetopause during periods of southward IMF. This convection is subject to adiabatic constraints during the slowly evolving growth phase, that is, the depletion of magnetic flux in the tail is confined to the region of flux tube entropy which matches the entropy of recently reconnected flux tubes on the dayside. The MFD leads to a strong reduction of B_z in a flux reservoir located in the midnight equatorial plane and results in strong CS thinning as well as a significant increase of the crosstail current. This thin CS is highly concentred near the equatorial plane and located within $x = -15\,R_E$ in the late growth phase, which suggests that an instability leading to magnetic reconnection onset is possibly in the near-Earth tail. Satellite observations also indicate that tailward plasma flows associated with local magnetic reconnections can occur in the near-Earth tail region [*Sergeev et al.*, 1995; *Petrukovich and Yahnin*, 2006].

This paper further examines the ionospheric dynamics associated with the changes of magnetotail structure by mapping tail properties from the earthward boundary into the ionosphere. Our results show that overall plasma sheet features move equatorward by 2 to 3° caused by the depletion of closed magnetic flux. Figure 12 illustrates the MFD process and the associated equatorward motion during the growth phase. The closed magnetic flux is removed by the sunward divergent convection in the near-Earth tail (red arrows in the equatorward plane) and therefore causes a contraction of the ionospheric footpoints of this tail region. The magnetic field line (a) located equatorward is approximately stationary, and the ionospheric footpoints of the magnetic field lines (b) and (c) converge toward lower latitudes even though their earthward motion in the tail is small. This convergent motion results in a sharp transition from the dipole to stretched magnetic field as well as strong CS thinning during the growth phase.

The results of MFD show that the sunward divergent flow is associated with the source region of field-aligned currents. The R1 and R2 currents are likely evolved associated with the changes of outer and inner boundaries of the return convection channel. In the late growth phase, magnetic field lines are highly deformed by a faster divergent convection in a narrower channel such that the strong field-aligned currents develop into a very thin region about 1° in latitude. Also, the R1/R2 boundary is approximately coincident with the electron isotropy boundary in the late growth phase. A plausible proxy of the preonset arc may be the location of the highest intensity R1 currents. The presented results suggest that this region is located in close proximity just poleward of the 100 keV electron IB and in close proximity to the intensified R2 currents.

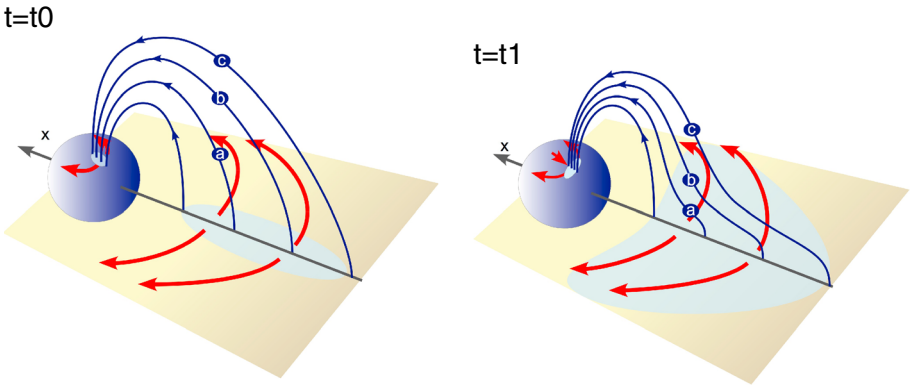

Figure 12. Illustration of midnight MFD process and the associated equatorward motion at the ionosphere at times (left) $t = t_0$ (initial) and (right) $t = t_1$ (growth phase). The points (a),(b), and (c) represent different magnetic field lines. The sunward divergent flow is presented as red arrows in the equatorward plane.

Our model results indicate that the distance between the maximum R1 intensity, the electron IB, and the R2 current is smaller than 1° toward the end of the CS thinning. Considering either the R2 current region or a small region poleward of the ion IB as proxies for ion precipitation, it is conceivable that the onset arc is either just poleward of the diffuse aurora or even within the region of diffuse proton aurora considering the several 10 km broadening of it by charge exchange collisions. This is consistent with results by *Newell et al.* [1998] which demonstrate that the 30 keV ion isotropy boundary corresponds well to the latitude of the maximum ion energy flux precipitation. These results agree well with many observational studies and may shed light on the controversy regarding the location of the late growth phase arc relative to the diffuse proton aurora.

The physics of substorm onset has been highly debated for some time, i.e., outside-in and inside-out models [*Baker et al.*, 1996; *Lui*, 1996]. The outside-in model proposes that near-Earth tail reconnection triggers the substorm onset and expansion by the injection and rapid earthward deceleration of fast flows, whereas the inside-out model suggests that a near-Earth instability triggers the substorm onset such that auroral expansion could proceed before the arrival of earthward directed fast flows at the boundary to the dipolar magnetosphere. The detailed observational confirmation of either model is not easy and depends heavily on the exact relative locations of satellites and ground observations. It is also not unambiguous because of the incomplete knowledge of the magnetospheric configuration which determines the mapping. Close to the end of the CS thinning in our simulation, field lines from 10 R_E and 20 R_E in the magnetotail (in the midnight meridian) map to the latitudes of 65.4° and 66.0°, respectively, which is less than 1° latitudinal separation in the ionosphere. The result suggests that the distinction between the inside-out and outside-in hypotheses is even more challenging than conventionally assumed, because the intense field-aligned currents and IBs develop in a very narrow latitudinal region which makes it difficult to attribute any ionospheric observations in this region to a magnetotail location between 10 and 20 R_E. A less than 1° separation is also well within the uncertainty of the mapping of traditional magnetic field models [*Shevchenko et al.*, 2010].

In summary, this paper examines the changes of the magnetotail structure mapped into the ionosphere during the growth phase based on a mesoscale tail simulation of magnetic flux depletion. The depletion is caused by azimuthal sunward flow out of the simulation domain with a flux transport rate of 40 kV. *Otto et al.* [2014] have examined the influence of different potential values. They found that the main effect of a different potential is a change of the temporal evolution, but the results are basically identical. Therefore, different potential or flux transport rates generate the same ionospheric signatures and mapping properties but on a different time scale $t \sim 1/\Phi$. Overall our results demonstrate an ionospheric equatorward motion about 2 to 3° associated with the evolution of CS thinning caused by the midnight MFD. The removal of magnetic flux in the near-Earth tail causes a contraction of the ionospheric footpoints of this tail region such that all of the mapped magnetotail quantities participate in the equatorward motion. It is found that the mapped thin CS is located in the region where magnetic flux is strongly depleted and in close proximity with strong and narrow R1 and R2 sense field-aligned currents which are separated by less than 1° in latitude at the end of the CS thinning. The presented results also show a sharp transition between the dipole and

stretched magnetic field and an evolution of thinning and convergent motion of field-aligned currents in the late growth phase.

All of the presented results have been obtained by considering only the depletion of closed magnetic flux in the midnight region without adding magnetic flux and energy to the lobes. The objective of this approach was to examine the effects of magnetic flux depletion, and including a lobe driver would have made it difficult or impossible to attribute configurational changes of the magnetotail or of the mapping to either cause. This does not imply that a lobe driver is unimportant for the evolution during the growth phase. It is well known that such a driver can also cause CS formation. Note, however, that a lobe driver alone can only locally redistribute the equatorial magnetic field in the tail such that the significant equatorward displacement of ionospheric boundaries likely requires significant magnetic flux depletion as considered in the presented results. The combined effects of closed flux depletion and lobe driving will be investigated separately.

Acknowledgments
The authors thank the reviewer for his/her helpful comments.

Masaki Fujimoto thanks the reviewer for his/her assistance in evaluating this paper.

References

Aikio, A. T., T. Lakkala, A. Kozlovsky, and P. J. S. Williams (2002), Electric fields and currents of stable drifting auroral arcs in the evening sector, *J. Geophys. Res.*, *107*(A12), 1424, doi:10.1029/2001JA009172.

Akasofu, S.-I. (1964), The development of the auroral substorm, *Planet. Space Sci.*, *12*, 273–282.

Asano, Y., T. Mukai, M. Hoshino, Y. Saito, H. Hayakawa, and T. Nagai (2003), Evolution of the thin current sheet in a substorm observed by Geotail, *J. Geophys. Res.*, *108*(A5), 1189, doi:10.1029/2002JA009785.

Baker, D. N., T. I. Pulkkinen, R. L. McPherron, J. D. Craven, L. A. Frank, R. D. Elphinstone, J. S. Murphree, J. F. Fennell, R. E. Lopez, and T. Nagai (1993), CDAW 9 analysis of magnetospheric events on May 3, 1986: Event C, *J. Geophys. Res.*, *98*, 3815–3834.

Baker, D. N., T. Pulkkinen, V. Angelopoulos, W. Baumjohann, and R. McPherron (1996), Neutral line model of substorms: Past results and present view, *J. Geophys. Res.*, *101*(A6), 12,975–13,010, doi:10.1029/95JA03753.

Birn, J., M. Hesse, and K. Schindler (1998), Formation of thin current sheets in space plasmas, *J. Geophys. Res.*, *103*, 6843–6852.

Bristow, W. A., G. Sofko, H. C. Stenbaek-Nielsen, S. Wei, D. Lummerzheim, and A. Otto (2003), Detailed analysis of substorm observations using SuperDARN, UVI, ground-based magnetometers, and all-sky imagers, *J. Geophys. Res.*, *108*, 1124, doi:10.1029/2002JA009242.

Clausen, L. B. N., J. B. H. Baker, J. M. Ruohoniemi, S. E. Milan, and B. J. Anderson (2012), Dynamics of the region 1 Birkeland current oval derived from the Active Magnetosphere and Planetary Electrodynamics Response Experiment (AMPERE), *J. Geophys. Res.*, *117*, A06233, doi:10.1029/2012JA017666.

Coroniti, F. V., and C. F. Kennel (1973), Can the ionosphere regulate magnetospheric convection?, *J. Geophys. Res.*, *78*(16), 2837–2851, doi:10.1029/JA078i016p02837.

Coroniti, F. V. (1985), Explosive tail reconnection: The growth and expansion phases of magnetospheric substorms, *J. Geophys. Res.*, *90*, 7427–7447.

Erickson, G. M., and R. A. Wolf (1980), Is steady convection possible in the Earth's magnetotail?, *Geophys. Res. Lett.*, *7*, 897–900.

Hesse, M., and J. Birn (1993), Three-dimensional magnetotail equilibria by numerical relaxation techniques, *J. Geophys. Res.*, *98*, 3973–3982.

Kan, J. R. (1990), Tail-like reconfiguration of the plasma sheet during the substorm growth phase, *Geophys. Res. Lett.*, *17*, 2309–2312.

Kokubun, S., and R. L. McPherron (1981), Substorm signatures at synchronous altitude, *J. Geophys. Res.*, *86*, 11,265–11,277.

Lee, L. C., L. Zhang, A. Otto, G. S. Choe, and H. J. Cai (1998), Entropy antidiffusion instability and formation of a thin current sheet during geomagnetic substorms, *J. Geophys. Res.*, *103*, 29,419–29,428.

Lui, A. T. Y. (1996), Current disruption in the Earth's magnetosphere: Observations and models, *J. Geophys. Res.*, *101*(A6), 13,067–13,088, doi:10.1029/96JA00079.

McPherron, R. L., C. T. Russell, and M. P. Aubry (1973), Satellite studies of magnetospheric substorms on August 15, 1968: 9. Phenomenological model for substorms, *J. Geophys. Res.*, *78*, 3131–3149.

Mozer, F. S. (1971), Origin and effects of electric fields during isolated magnetospheric substorms, *J. Geophys. Res.*, *76*(31), 7595–7608, doi:10.1029/JA076i031p07595.

Newell, P. T., V. A. Sergeev, G. R. Bikkuzina, and S. Wing (1998), Characterizing the state of the magnetosphere: Testing the ion precipitation maxima latitude (b2i) and the ion isotropy boundary, *J. Geophys. Res.*, *103*(A3), 4739–4745, doi:10.1029/97JA03622.

Ohtani, S., S. Wing, P. T. Newell, and T. Higuchi (2010), Locations of night-side precipitation boundaries relative to R2 and R1 currents, *J. Geophys. Res.*, *115*, A10233, doi:10.1029/2010JA015444.

Otto, A. (1990), 3D resistive MHD computations of magnetospheric physics, *Comput. Phys. Commun.*, *59*, 185–195.

Otto, A., M.-S. Hsieh, and F. Hall (2014), Current sheet formation in planetary magnetotails, in *Magnetotails in the Solar System*, in press.

Petrukovich, A. A., and A. G. Yahnin (2006), The substorm onset location controversy, *Space Sci. Rev.*, *122*, 81–87.

Petrukovich, A. A., W. Baumjohann, R. Nakamura, A. Runov, A. Balogh, and H. Rème (2007), Thinning and stretching of the plasma sheet, *J. Geophys. Res.*, *112*, A10213, doi:10.1029/2007JA012349.

Saito, M. H., D. Fairfield, G. Le, L. N. Hau, V. Angelopoulos, J. P. McFadden, U. Auster, J. W. Bonnell, and D. Larson (2011), Structure, force balance, and evolution of incompressible cross-tail current sheet thinning, *J. Geophys. Res.*, *116*, A10217, doi:10.1029/2011JA016654.

Sanny, J., R. McPherron, C. Russell, D. Baker, T. Pulkkinen, and A. Nishida (1994), Growth-phase thinning of the near-Earth current sheet during the CDAW 6 substorm, *J. Geophys. Res.*, *99*(A4), 5805–5816, doi:10.1029/93JA03235.

Schindler, K., and J. Birn (1993), On the cause of thin current sheets in the near-Earth magnetotail and their possible significance for magnetospheric substorms, *J. Geophys. Res.*, *98*(A9), 15,477–15,485, doi:10.1029/93JA01047.

Sergeev, V. A., and N. A. Tsyganeznko (1982), Energetic particle losses and trapping boundaries as deduced from calculations with a realistic magnetic field model, *Planet. Space Sci.*, *30*, 999–1006.

Sergeev, V. A., P. Tanskanen, A. Korth, and R. C. Elphic (1990), Current sheet thickness in the near-Earth plasma sheet during substorm growth phase, *J. Geophys. Res.*, *95*, 3819–3828.

Sergeev, V. A., M. Malkov, and K. Mursula (1993), Testing the isotropic boundary algorithm method to evaluate the magnetic field configuration in the tail, *J. Geophys. Res.*, *98*, 7609–7620.

Sergeev, V. A., V. Angelopoulos, D. G. Mitchell, and C. T. Russell (1995), In situ observations of magnetotail reconnection prior to the onset of a small substorm, *J. Geophys. Res.*, *100*, 19,121–19,133.

Sergeev, V. A., Y. Nishimura, M. Kubyshkina, V. Angelopoulos, R. Nakamura, and H. Singer (2012), Magnetospheric location of the equatorward prebreakup arc, *J. Geophys. Res.*, *117*, A01212, doi:10.1029/2011JA017154.

Shevchenko, I. G., V. Sergeev, M. Kubyshkina, V. Angelopoulos, K. H. Glassmeier, and H. J. Singer (2010), Estimation of magnetosphere-ionosphere mapping accuracy using isotropy boundary and THEMIS observations, *J. Geophys. Res.*, *115*, A11206, doi:10.1029/2010JA015354.

Tsyganenko, N. A. (1996), Effects of the solar wind conditions on the global magnetospheric configuration as deduced from data-based models, in *Proceedings of 3rd International Conference on Substorms (ICS-3)*, edited by E. J. Rolfe and B. Kaldeich, pp. 181–185, ESA-SP–389, European Space Agency, Versailles, France.

Wang, C.-P., L. Lyons, T. Nagai, and J. Samson (2004), Midnight radial profiles of the quiet and growth-phase plasma sheet: The Geotail observations, *J. Geophys. Res.*, *109*, A12201, doi:10.1029/2004JA010590.

Xing, X., L. Lyons, Y. Nishimura, V. Angelopoulos, D. Larson, C. Carlson, J. Bonnell, and U. Auster (2010), Substorm onset by new plasma intrusion: THEMIS spacecraft observations, *J. Geophys. Res.*, *115*, A10246, doi:10.1029/2010JA015528.

Yahnin, A., V. A. Sergeev, B. B. Gvozdevsky, and S. Vennerstrom (1997), Magnetospheric source region of discrete auroras inferred from their relationship with isotropy boundaries of energetic particles, *Ann. Geophys.*, *15*, 943–958.